Progress In Electromagnetics Research, PIER 39, 125–145, 2003

COMPRESSION OF POLARIMETRIC SYNTHETIC APERTURE RADAR DATA

S. El Assad, X. Morin, and D. Barba

Ecole polytechnique de l'université de Nantes
Rue Christian Pauc BP 50609, Nantes Cedex 3, France

V. Slavova

New Bulgarian University
21 rue Montevideo, 1635, Sofia, Bulgaria

Abstract—The paper deals with proposition and evaluation of new and specific methods to represent vector radar data acquired by means a side-looking measurement in order to use compression process of Lind, Buzo, Gray (LBG), and Kohonen's self organizing feature maps of topology. The aim is to enable after coding, transmission, and decoding a high-resolution reconstruction image using the Synthetic Aperture Radar (SAR) methods. The approach proposed for compression uses the statistical properties of the signals to be compressed in order to perform the vector quantification in an optimal way.

1. INTRODUCTION

The recent image systems grow to be of high performance because of their ability of acquisition of multi-polar and multi frequency data. By using various combinations of horizontal and/or vertical polarization configurations of the transmission and reception ends, the complete polarimetric scattering matrix is measured for each resolution element of the imaged scene. These systems permit to increase the capcity of interpretation of radar signals and to use another class of methods for speckle reduction, classification and compression of vectorial data relating to physical proporties of natural targets.

SAR processing requires substantial computation because of the large-amount of data acquired by the system. The usual size, weight and power limitations of many space-and airborne SAR platforms preclude on-board SAR processing. Rather, the radar returns are transmitted to SAR processing facilities on the ground. Transmission of these data over limited bandwidth channels requires the data to be compressed. The degree of compression required necessitates the use of lossy compression techniques. These compression algorithms are applied before any further processing is done on the data and all target reconstruction, detection and recognition is done on an approximation of the original data generated by the decoding algorithm.

Given a representation accuracy, the performance of compression algorithms is higly depends on the statistical properties of the signals to be coded and on their dynamics range.

For this reason, we carry out a detailed analysis of these properties and demonstrate that it is very important for the methods of vector quantization to take into consideration the correlation between the vector components. We validate our approach by applying it on real data acquired a lateral sighting device: the system STRADI_VL, a full polarimetric (H-V basis) multi-band sensor developed by CELAR (Centre d'Electronique de l'Armement) for physical study of clutter backscattering.

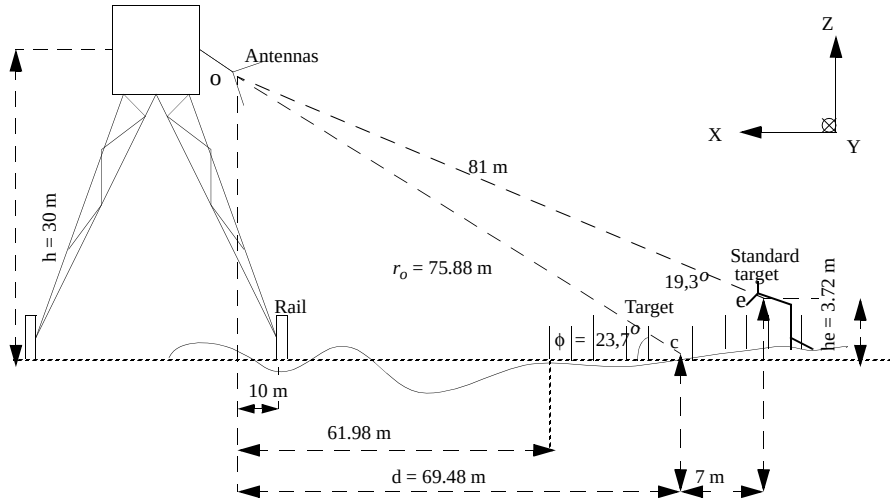

Figure 1. STRADI_VL Geometric configuration for measurements.

The organization of this paper is as follows: a description of the device and signals measured are presented in Section 2. In Section 3, several statistical properties are examined and analyzed: average, variance, distribution of the data, correlation of frequencies and positions of the radar, and correlation between channels of polarization. Section 4, described the two methods of compression developed and tested: the vectorial quantification (QV) based on designing of codebook (modified algorithm LBG) and networks of Kohonen before concluding.

2. DESCRIPTION OF THE MEASUREMENT DEVICE STRADI_VL AND OF THE CHOSEN SCENES

The radar is fixed on a high (30 meters) metallic tower. This structure is able to move ahead and backward on a 200 meters rail, along the Y axis (Figure 1). The lateral scanning used here is 333 cm with steps of 3 cm (i.e., 111 positions). The geometric configuration makes possible to observe scenes covered by the angle interval between 55° and 10°. The data collection system used is multi-frequency and multi-polarization.

For each radar position, the emitted signal is synthesized frequency by frequency for one given polarization (H or V), after that applied simultaneously on the modules of emission and reception in order to insure that the module of reception keeps a coherent reference

(amplitude and phase). The back-scattering signal is received into two orthogonal antennas, one horizontal, the other vertical and processed independently in separate channels. The four terms of the scattering matrices (HH, VH, VV and HV) can then be formed by alternating the polarization of the emitted signal for each position of the radar.

For each term of this matrix, the acquired signal is presented as a two-dimensional table 'position-frequency'. The first dimension consists in a set of positions of the radar (cadence of impulses) and the second — the frequency response for a ramp of frequencies included between 8.5 and 9.5 Ghz (the X band) with a step of 2 Mhz (i.e., 501 frequencies by position are emitted). The size of the scene, which can be treated, is 25.6 meters long and 12.8 meters large. The pixels size is 10 cm×10 cm.

The set of these measurements makes up a hologram. The image reconstruction is based on "Holagraphic SAR Image Formation by Coherent Summation of Impulse Responses Derivatives" [2, 3].

2.0.1. Presentation of the Treated Scenes

Five scenes have been measured by 'STRADI_VL' and have been used in this study. The first one involves a car — a Peugeot 305 (file '305'), hidden in a field of corn (maize — 210 cm high). There are one small area covered with herbs and one concrete plate of approximately 9 m2 on the foreground of the scene. A mask has been applied for the most part of the pixels, representative for the car.

The second scene consists in a hybrid roof (file 'roof'), one half made of schist slates and the other half covered with clay tiles. This construction is arranged on a floor made of both concrete and asphalt. The plane surface covered by schist slates and clay tiles is in the specular direction of the radar line of sight.

The third decor (file 'fallow land') consists mostly in trees with deployed leaves and in a small part (25% of the area) — of not cultivated ground on which there are visible some small shrubs. The fourth panorama (the file 'sand') contains an area of artificial sand on which they are assembled three walls made of stone blocks. The background consists in a field of corn (maize — 210 cm tall).

At least, the fifth scene, which has been used (file 'parcel'), represents a parcel, quite nude, on which one sandy surface and one small rectangular field of ground are seen.

The aggregation of the five described files contains 278055 complex signal instances in total. They represent a data collection from cases, diversified and representative for the diffusion of electromagnetic waves passing a patch and rural scenes.

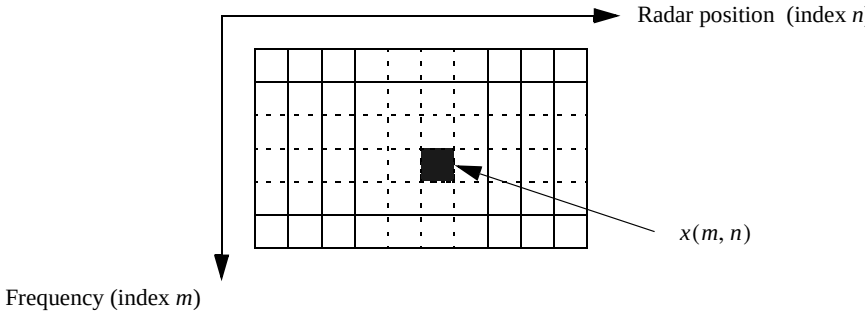

Figure 2. Two-dimensional raw signal measured by the radar system.

3. RADAR SIGNAL STATISTICS

As the performance of compression methods is highly dependent on the statistical properties of the acquired signals, we have investigated these properties for the gathered data collection. The result of the statistical study is given bellow. The accent is centered on the correlation for the diverse configurations of polarization.

It is difficult to enumerate the various possible manners for constructing vectors. We have chosen to reduce the investigation on vectors that consist in 6 real components. This choice is explained, after that a complete balance of the correlations associated to each of the vectors is made.

When radar illuminates a scene, it also captures a fraction of the backscattered field from the entire set of objects, which are in the lobe of the antenna. The response received from one resolution cell (zone on the ground which contributes to the measured signal with one pixel) is the sum of L responses of separate independent scatterers, randomly distributed in the cell. That is why, the complex value of one pixel of the 2D table of received signals of Figure 2 is [12]:

$$x(m,n) = \sum_{k=1}^{L} \rho_k \exp(j\phi_k) = I + jQ \tag{1}$$

with: ρ_k is the reflectance amplitude and ϕ_k is the phase delay which is a function of signal wavelength, path distance and of any scatterer proper phase. The amplitude ρ_k and the phase ϕ_k are assumed to be statiscally independent of each other and of the amplitude and phase of any other elementary phasor. Moreover, the scatterers have in principle unknown range, so ϕ_k are supposed to be independent of each other and uniformly distributed in the interval $[0, 2\pi]$. Therefore, real

and imaginary parts of the complex signal have zero means, identical variances, and are uncorrelated. It follows from this statement that the corresponding amplitude is Rayleigh distributed, while the phase is a uniform random variable. In that case, optimal algorithms can be used for compression purpose.

3.1. Means and Variances

The estimation of the two statistics — mean and standard deviation of the received signals give knowledge about the energy and the dispertion of the signal. The mean is simply:

$$E\{x(m,n)\} = \frac{1}{MN} \sum_{m=1}^{M} \sum_{n=1}^{N} x(m,n) \tag{2}$$

The standard deviation is as follows:

$$\sigma(x) = \sqrt{E\{x_c(m,n)x_c^*(m,n)\}} \tag{3}$$

with:

$$x_c(m,n) = x(m,n) - E\{x(m,n)\} \tag{4}$$

the centered value of a pixel.

The following tables show the received signal means and standard deviations of files '305' and 'roof'. The associated suffix gives information about the polarization channel under study (for example, "VH" means that the transmitted signal is vertically polarized, while the received signal is measured in the horizontal polarization channel).

It comes out from the tables that the energy contained in the raw signal data of the file '305' is 2.2 times higher than the energy contained in the raw signal in the file 'roof'. This could be explained with the clutter density, which is higher in the first scene (maize). The clutters of the objects in the second scene, except those of the roof, are in general not in the specular direction (reflector disposition) of the line sight radar. The complex signals are approximately centered in the cross-polarized channels (HV and VH). On the contrary, in the channels of co-polarization (HH and VV) the imaginary part of the signal seams to have a mean close to zero. The co-polar to cross-polar ratio (powers, received in the co-polarized 'direct' channels and those, measured in the cross-polarized channels) is between 1.2 and 1.4.

The mean of modules (the 'amplitude') is 1.5 to 2 times higher in the co-polarized channels than in the cross-polarized channels. The ratio between the means of the correspondent modules in the two data files is very close to one. The standard deviation of the modules is

Table 1. Mean and standard deviation of the complex measured signal.

$x(m,n)$	305_HH	305_VV	305_VH	305_HV	toit_HH	toit_VV	toit_HV	toit_VH
mean	14.274 $+j0.018$	14.306 $-j0.015$	-0.065 $+j0.188$	0.204 $+j0.188$	14.224 $+j0.014$	14.215 $+j0.004$	-0.272 $+j0.054$	-0.008 $-j0.317$
standard deviation	14.977	14.745	12.247	12.247	9.754	9.449	8.687	8.714

Table 2. Mean and standard deviation of modules.

Module	305_HH	305_VV	305_VH	305_HV	toit_HH	toit_VV	toit_HV	toit_VH
mean	18.706	18.634	11.861	11.882	16.241	15.945	8.448	8.464
standard deviation	8.841	8.664	2.936	2.980	5.804	6.092	2.046	2.093

Table 3. Mean and standard deviation of phases.

Phase (°)	305_HH	305_VV	305_VH	305_HV	toit_HH	toit_VV	toit_HV	toit_VH
mean	-0.426	-0.572	0.747	-1.040	-0.572	-1.253	0.072	-2.258
standard deviation	53.883	54.359	104.358	103.467	33.790	31.591	105.044	103.935

Table 4. Mean and standard deviation of real parts.

Real part	305_HH	305_VV	305_VH	305_HV	toit_HH	toit_VV	toit_HV	toit_VH
mean	14.274	14.306	-0.065	0.204	14.224	14.215	-0.272	-0.008
standard deviation	10.587	10.413	8.659	8.658	6.404	6.529	6.141	6.164

Table 5. Mean and standard deviation of imaginary parts.

Imaginary part	305_HH	305_VV	305_VH	305_HV	toit_HH	toit_VV	toit_HV	toit_VH
mean	0.012	-0.015	0.189	-0.188	0.014	-0.004	0.054	-0.317
standard deviation	10.594	10.447	8.661	8.662	7.358	6.834	6.145	6.159

about 3 times higher in the co-polarized channels. The corresponding standard deviations from the identical channels are also close enough to each other. The coefficient of variation (the ratio between the standard deviation and the mean) of the amplitudes is twice higher for the co-polarized direct channels than in the cross-polarized ones in both data files.

In both data files the phases are centered and have high standard deviation. It is 2 to 3 times higher the cross-polarization the direct channels. However, it is difficult to obtain a mean and a standard deviation of the phase as this parameter involves ambiguities 2π.

3.2. Histograms

The histograms obtained from the two data files — '305' and 'roof' are shown on the Figure 3 — the amplitudes, the phases and the real parts of the signal. The shown histograms are built for a selection of couples of polarization 'emission-reception'.

In cross-polarization, the phase tends to a uniform distribution and the amplitude has a Gauss-like profile. The case is not the same in co-polarization where both — amplitude and phase seam tending to some not uniform behavior. For the file '305' the amplitude is like to be a superposition of two separate and distinguishable lows on the histogram curves. The reason for this result could be in the 'nature' of the source phenomenon — two accurately separable sets of objects with quite different scatters are on the scene '305' — the car and the calibration references on one hand, and the corn patch on the other.

We have applied the test of convergence of Smirnov-Kolmogorov, considered as appropriate for such cases of data, based on the measure of the maximal distance between the cumulated densities of the statistically obtained characteristics of acquired data and those of the supposed theoretical low of distribution. The theoretical lows of distribution, which have been tested, are the Gauss normal distribution, the distributions of Rayleigh, Weibull, Rice, the logarithmic, Gamma and K distributions.

The result, obtained with the Smirnov-Kolmogorov test, indicates that in general none of the mentioned lows fit to the statistical data. Certain curves have Gauss-like profile. More precisely, when the amplitude is Gauss-shaped curve, the phase tends to a uniform distribution (cross-polarized channels). Following a kind of mirror analogy, when the phase tends to a Gauss-shaped curve, the amplitude seems to 'enlarge' (co-polarized channels).

The theoretical curves are shown on the histograms with bold lines — Rayleigh distribution law for the amplitude and Gauss distribution law for all the other histograms.

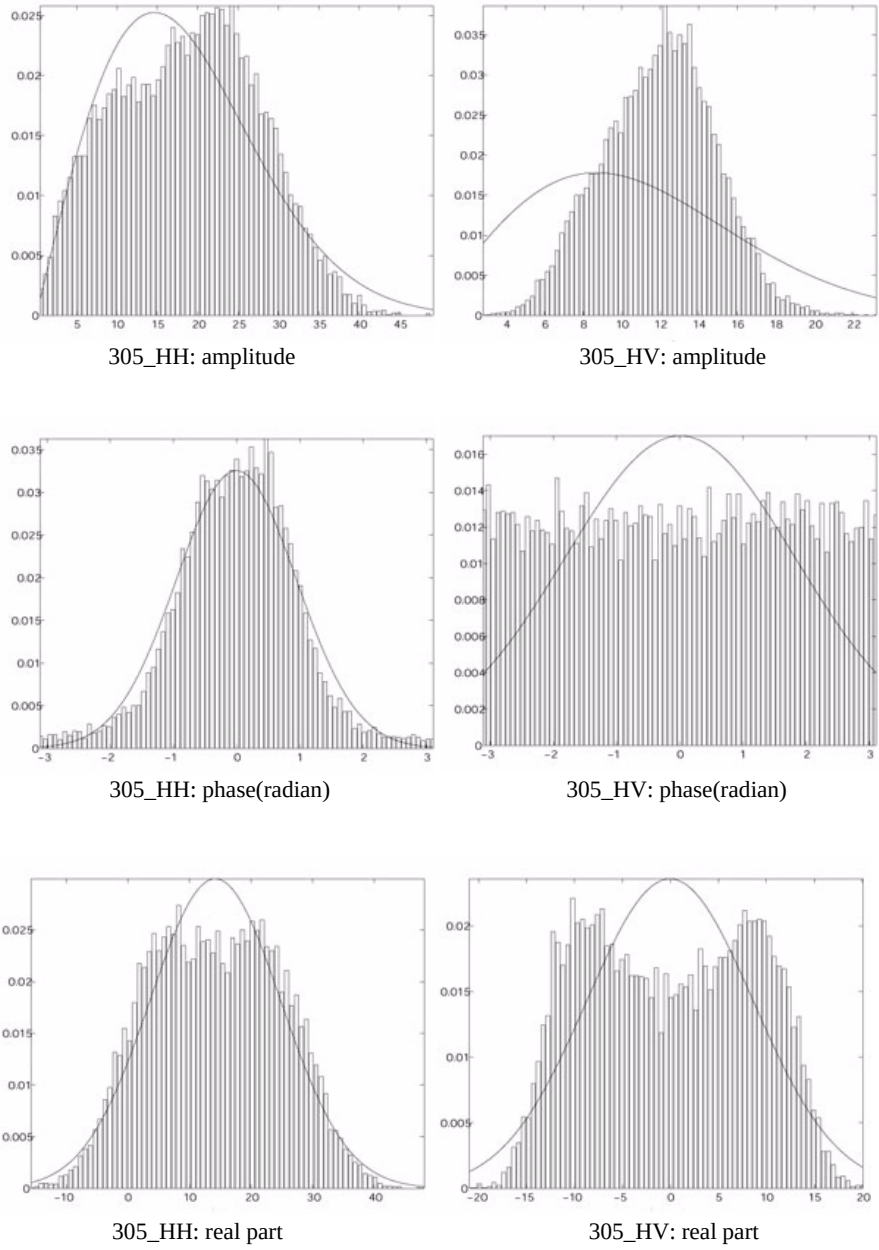

Figure 3a. Histogram measured in the HH and HV channels: file car 305.

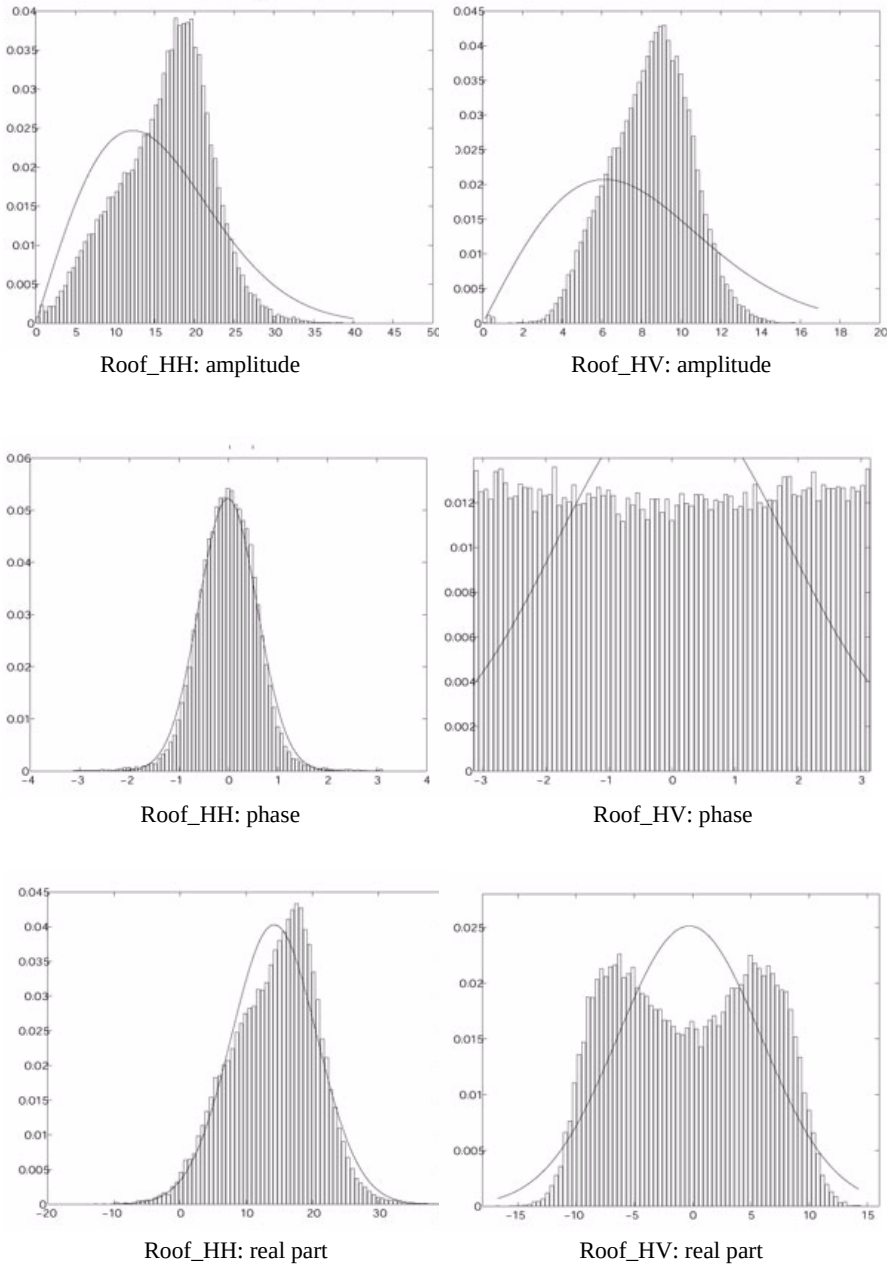

Figure 3b. Histogram measured in the HH and HV channels: file roof.

3.3. Auto-correlation and Inter-correlation

In this paragraph, the auto-correlation properties of the raw signal depending on frequency and lateral displacement are examined. The frequency auto-correlation of the raw signal indicates how the variations of the received signal depend on the changes of the emitted signal frequency. The statistical result is calculated as an average of all correlations, resulting from each position of the imaging system. In the same way, the lateral displacement correlation expresses how the signal variations depend on the changes of the metallic tower's position. The results obtained for each frequency are then averaged.

The inter-correlation between polarization channels is also calculated. It allows evaluating the rapidity of variation of signal from one channel to another.

3.3.1. Autocorrelation of the Acquired Raw Signal

The registered signal $x(m,n)$ in one of the polarization channels (HH, HV, VH, VV) is not a direct function of the time but of the emitted frequency and of the position of the acquiring system. Consequently, the frequency autocorrelation of the measured signals is defined as follows:

$$C_f(l) = \frac{M}{M-|l|} \frac{\sum_{m=1}^{M}\sum_{n=1}^{N} x_c(m,n)x_c^*(m+l,n)}{\sum_{m=1}^{M}\sum_{n=1}^{N} x_c(m,n)x_c^*(m,n)} \tag{5}$$

The term $\frac{M}{M-|l|}$, a factor of balance, is intended to compensate the decrease of number of calculations performed when $|l|$ increases. The denominator is the variance of the signal.

Similarly, the autocorrelation in lateral displacement is given with the following expression:

$$C_d(l) = \frac{N}{N-|l|} \frac{\sum_{m=1}^{M}\sum_{n=1}^{N} x_c(m,n)x_c^*(m,n+l)}{\sum_{m=1}^{M}\sum_{n=1}^{N} x_c(m,n)x_c^*(m,n)} \tag{6}$$

These expressions take into account the complex form of the acquired signal. The calculation of correlation may also be applied to the module, to the phase, to the real or imaginary parts of the signal.

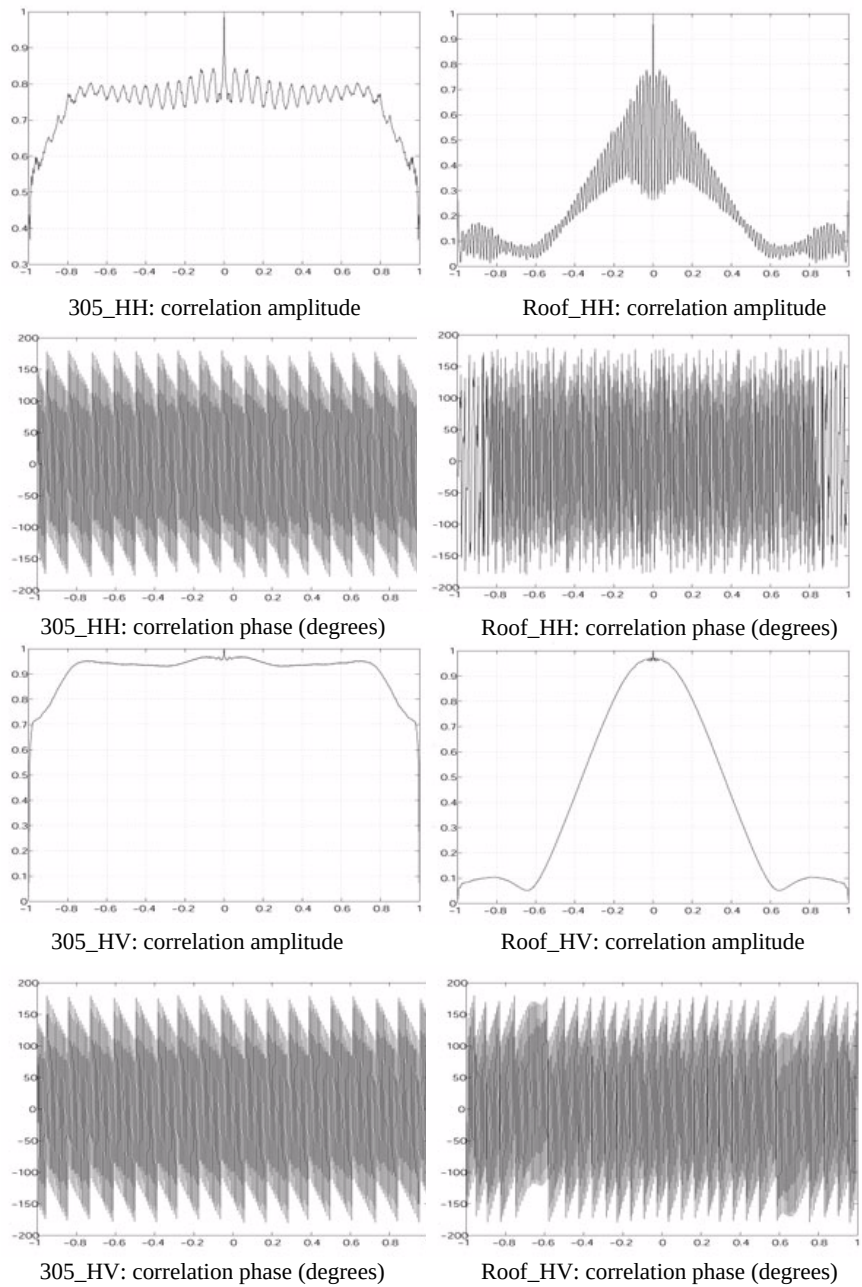

Figure 4. Autocorrelation function of the received signal versus the frequency shift (GHz).

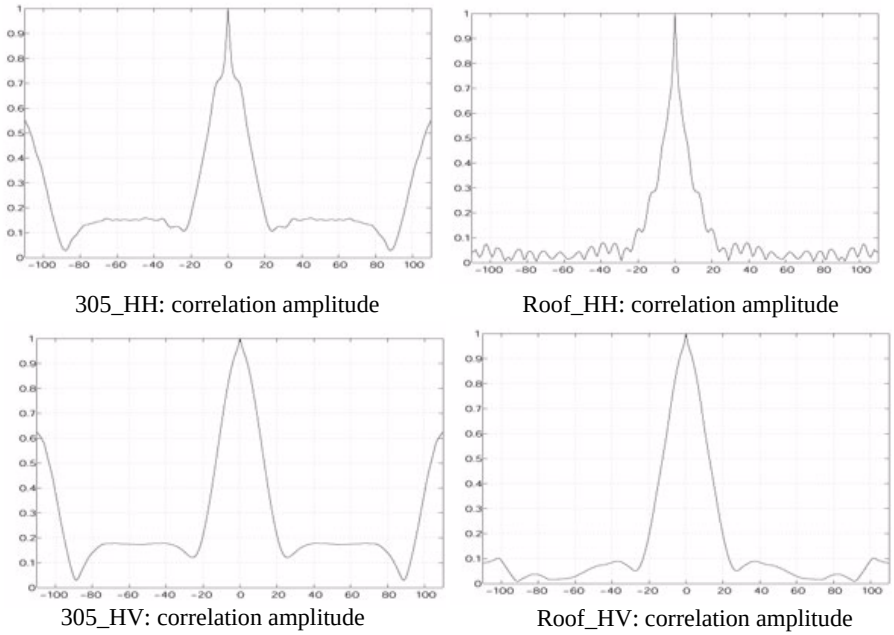

Figure 5. Autocorrelation function of the received signal versus the system displacement.

Because of the big number of the acquired curves, only one set of figures is presented. They are representative from the point of view of the interpretation of result. Although the vectors, manipulated for the vector quantization are constructed by specific entities (module, phase, real or imaginary parts), we expose essentially the results obtained from the complex signal, which is richer in information (Figs. 4, 5). After that we show the coefficient of correlation ρ for the set of manipulated quantities. It corresponds to a well determined element of the correlation function. It is the pixel to pixel correlation. So, following the frequency axis $\rho_f = C_f(l)$ and on the axis of displacement $\rho_d = C_d(l)$.

The module of the frequency correlation function decreases in a noticeable way at the very end of the frequency band. This fact can be observed for the various scenes. The correlation of frequency from the scene '305' is strong and containing some oscillations in direct polarization. The signals contained in the scene 'roof' are less correlated. The reason could be the homogeneous nature of the observed scene. In fact, each reflected signal is a global response of the illuminated with a monochromatic wave scene. It was expectable

to find out that the mean of the responses has a low sensibility for the frequency changes, as the heterogeneous environment (the maize), contains a big number of clutters, independently end randomly contributing to the response. The frequency correlation is stronger for the cross-polarized channels (HV and VH) then in the direct channels (VV and HH).

The decrease of the correlation with regard to the pick in lateral displacement is less rapid although the vision angle is modified. However, the distance between two acquisitions is here insufficient and has not enough influence on the global response from the scene about a given frequency. A considerable part of the received energy at the end of the course of the measurement appliance originates from the secondary lobes of the antennas, a fact which explains the increasing of correlation. It is evident that the presence of calibration devices has a dominating influence on the statistics of the received signals. The corresponding scenes sometimes seams to typical decors such as airports and urban zones.

3.3.2. Inter-correlation

The question is whether to evaluate in what extent the different polarization channels are correlated between each other. The parameters are the same as in the previous case: the frequency and the lateral displacement. The frequency inter-correlation function between the channels of polarization y and z (with: $y, z \in [HH, VV, HV, VH]$) is:

$$C_f^{yz}(l) = \frac{M}{M-|l|} \frac{\sum_{m=1}^{M} \sum_{n=1}^{N} x_{cy}(m,n) x_{cz}^*(m+l,n)}{\sigma(x_{cy})\sigma(x_{cz})} \tag{7}$$

Similarly, the inter-correlation in lateral displacement is:

$$C_d^{yz}(l) = \frac{N}{N-|l|} \frac{\sum_{m=1}^{M} \sum_{n=1}^{N} x_{cy}(m,n) x_{cz}^*(m,n+l)}{\sigma(x_{cy})\sigma(x_{cz})} \tag{8}$$

where $\sigma(x_{cy})$ and $\sigma(x_{cz})$ are the respective standard deviations of the complex random variables x_{cy} and x_{cz}. We are particularly interested in inter-correlation coefficients from set to set: $\rho = C_f^{yz}(0)$ or $\rho = C_d^{yz}(0)$, or in the inter-correlation coefficients of pixel to pixel: $\rho = C_f^{yz}(1)$ or $\rho = C_d^{yz}(1)$.

The Figures 6 and 7 show the obtained results. These lasts show that in frequency correlation, the oscillations are considerable

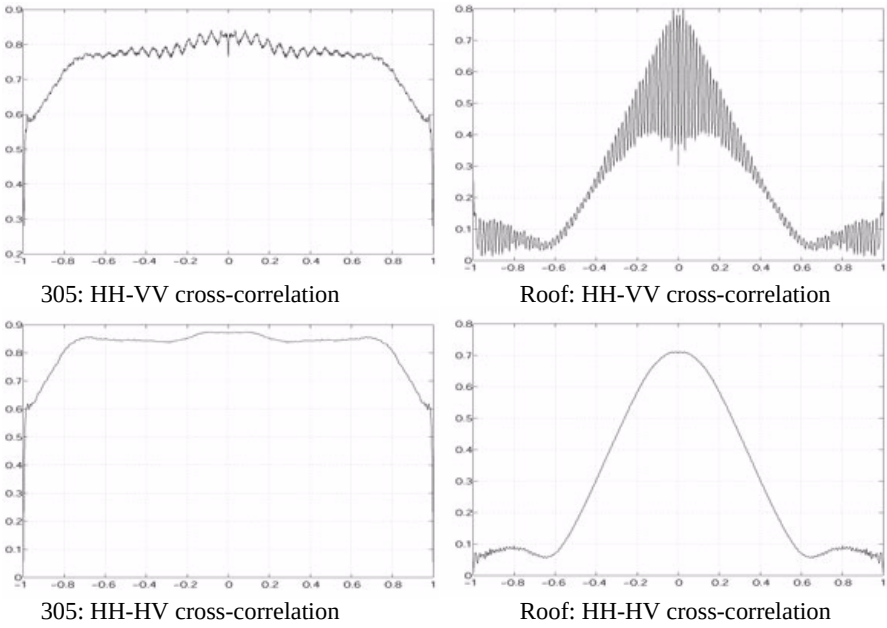

Figure 6. Cross-correlation amplitude for some channels versus the frequency shift (GHz).

between channels HH/HH, VV/VV and HH/VV. The last combination corresponds to the smallest inter-correlation between the calculated ones. The inter-correlation between the HV and VH channels is the stronger one. This is foreseeable because the acquisitions in the four channels are roughly simultaneous. The inter-correlations HH/VH and HH/VV (the same for VV/VH and VV/HV) are similar.

The same phenomenon of increasing at the end of displacement amplitude is observed in lateral inter-correlation. The calculated inter-correlation for the couple HH/VV of the scene 'roof' is approximately twice smaller then this, evaluated for the scene '305'. Apart this combination, it can be noticed that the profile of the inte-correlation module is almost independent in regard of the couple of considered polarization.

3.3.3. Outcome of Correlations Analyses

We present in Figure 8 a complete outline of the calculated means of correlation coefficients concerning the real and the imaginary parts of signals. On the figure is presented the average of the correlations

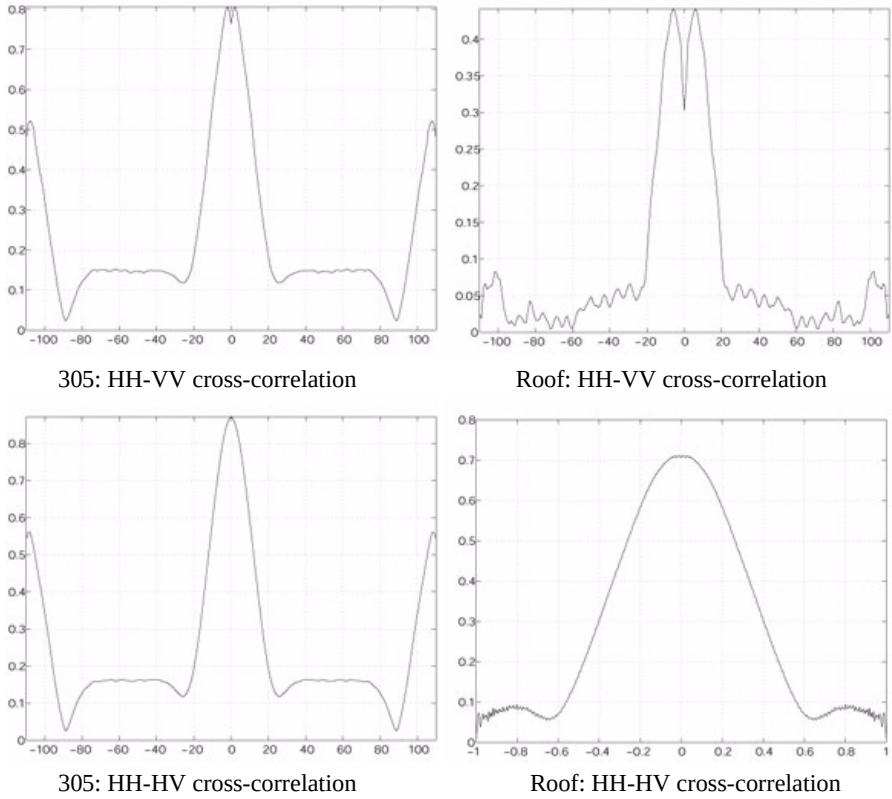

Figure 7. Cross-correlation amplitude for some channels versus the system displacement.

calculated independently for each data file.

4. DEVELOPED AND EVALUATED METHODS OF COMPRESSION

The used techniques of compression belong to the vector quantization methods. The vectors with 6 real components (6 adjacent real or imaginary parts of signal) are constructed as it is indicated on Figure 8. The preliminary treatment is intended to reduce the rate of transmission and results in higher cost of the treatment complexity. We have evaluated the performance of two types of compression algorithms: the LBG algorithm and the Kohonen's Self Organizing Feature Maps. We are interested especially in finding the

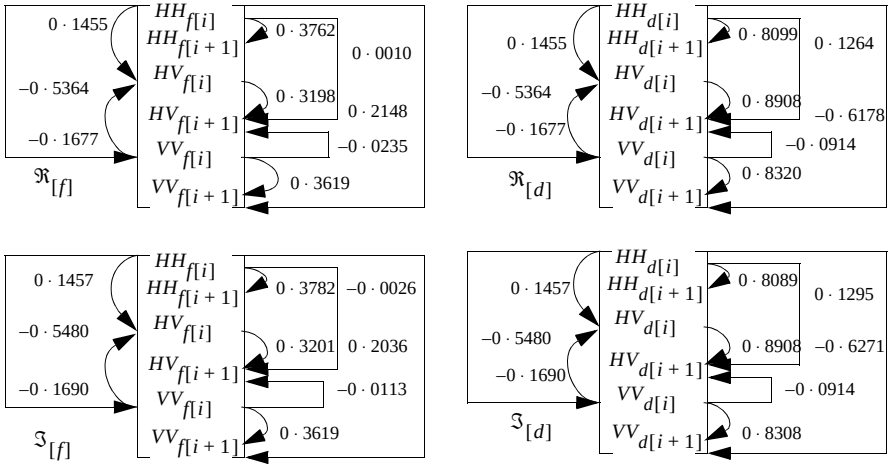

Figure 8. Correlation coefficients between elements of the constructed vector.

convenient compromise between the distortion (the ratio signal to noise of quantification) and the entropy, which predetermines the rate of numerical data. Before the compression, each component of the real signal is encoded on 32 bits. The rates we have desired to attend are lower then 2 bits per component.

4.1. LBG Algorithm

This algorithm is one, following from the K-means method. It assigns a representative (codeword) for each of the vectors to be coded. The operation is usually accomplished by minimizing the average error power between the data and their representatives, using L_2 norm. Only the index of the closest to the vector representative is transmitted. A codebook, consisting in the set of all representatives, is used. The performances of this type of coder are improved when the components of the vector are correlated. When using the usual K-means method, the number of codewords in the codebook is chosen a priori and the obtained clusters have a hyperspherical shape because of the used L_2 norm. The use of the Unsupervised Optimal Fuzzy Clustering Algorithm allows the use of an exponential norm and thus building clusters of any shape [7]. Moreover, it brings a solution to the problem of the optimal number of classes. The learning sequence of the codebook is formed by 100000 vectors, consisting only of the real parts of the signal. As the set of imaginary parts possess the same

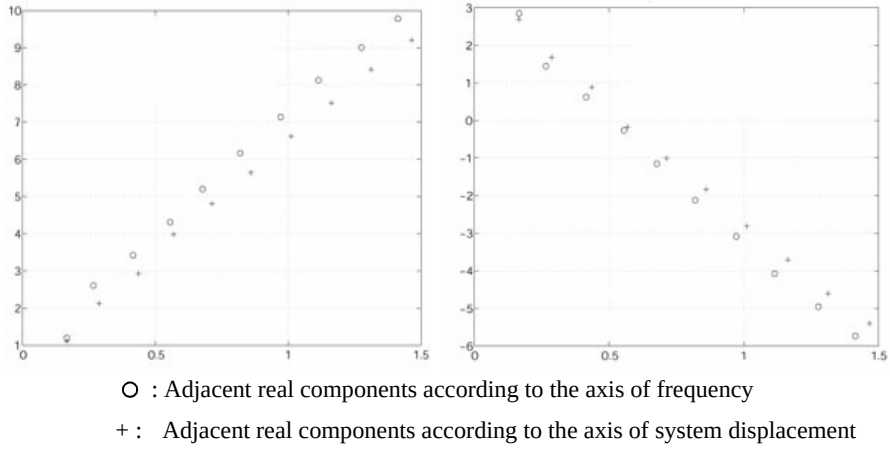

Figure 9. LBG algorithm: Distortion (dB) (left) and S/B (dB) versus the entropy by real component.

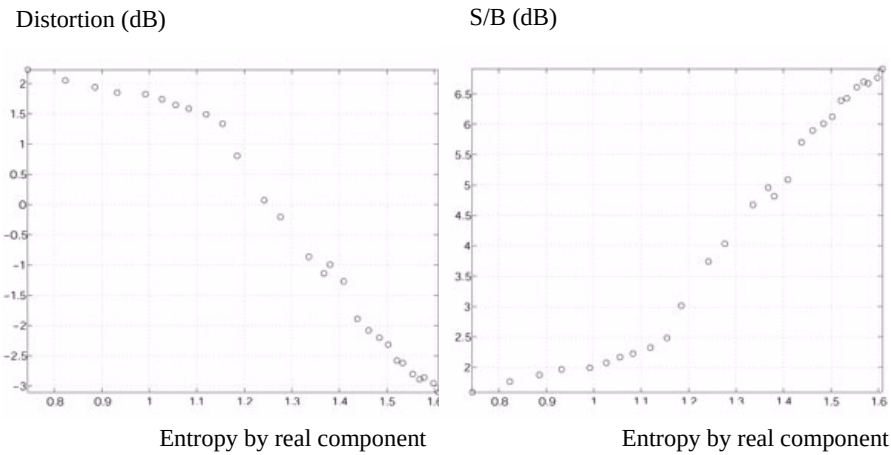

Figure 10. Kohonen's Self Organizing Feature Maps.

statistical characteristics, this same codebook is used later for coding the imaginary parts of the signal. That is one considerable advantage of the use of the proposed vector representation in comparison with the use of module and phase of signals. When modules and phases are used, the entire creation of two codebooks is unavoidable — the application of one and the same codebooks is not possible, as the statistical characteristics of the two entities are very different. A test sequence of 2000 vectors is used.

4.2. The Kohonen's Self Organizing Feature Maps

The Kohonen's Self-Organizing Feature Map (SOFM) is a neuron network with unsupervised learning which discovers alone some regularities in the input space and maps the spatial organization of the input patterns into spatial organization of the output nodes. During the learning procedure each node (neuron) of the network becomes 'sensible' to a class of input vectors. The learning is based on a sequence of input examples, submitted on the network's entry. Learning consists in choosing, for each input vector, the neuron with the closest to the vector weight and in tuning not only the winner, but also its spatial neighbors (with radius of neighborhood decreasing over time). This forces neighboring nodes to have similar 'receptive fields' (i.e., similar weight vectors) and leads to an internal representation, which corresponds to the structure of the source data. SOFM learns to categorize input vectors and learns also their distribution. Like in the case of the LBG algorithm, only the real parts of the vectors are used for the network training. The real and imaginary parts of the signal are after that coded by a simple assessment. The SOFM we have applied has a grid topology, with connected borders, i.e., the border neurons are connected with as many of nodes as those in the center of the square. The dimension of each neuron is 6.

Figures 9 and 10 show the obtained results in terms of distortion and signal-to-noise ratio. Compared to those obtained using the LBG algorithm, the performances of Kohonen are near 1.5 dB lower in terms of ratio signal to quantification noise for equal entropy. However, the Kohonen nets represent a good compromise between performances and calculation costs.

5. CONCLUSION

Some compression methods require a very good knowledge of the statistical behaviour of the data to be encoded. The first part of this paper is devoted to the study of the signal moments of order 0 and 1, and to their probability density functions. In the open literature, raw SAR signal amplitude and phase are assumed to be well-modelled respectively by a Rayleigh and a uniform distribution. To measure the veracity of this model on our own data, we used a reliable test of confidence. The results show that the signal can not be modelled by a simple distribution. This situation is due to the reconstruction method used (Lateral Holography). However, the use of lateral holography method cause the data to be highly correlated. That is the point that we exploited, the diverse correlations in the signal are of use when

constructing vectors and engender a considerable amelioration of the performances of the applied compression methods.

ACKNOWLEDGMENT

The authors are gratefully indebted to F. Fayar, P. Grandclement and J. C. Motet from the CELAR (Centre Electronique de l'Armement), for their technical support and the provision of STRADI_VL radar signal.

REFERENCES

1. Morin, X., "Caractérisation statistique de signaux de type ROS. Application au codage avec compression d'information," Thèse de Doctorat à l'ireste, Novembre 1997.
2. El Assad, S., I. Lakkis, and J. Saillard, "Holographic SAR image formation by coherent summation of impulse response derivatives," *IEEE Transactions on Antennas and Propagation*, Vol. 41, No. 5, 620–624, May 1993.
3. El Assad, S. and I. Lakkis, "An approach to radar imaging using the spherical projection density concept," *Annales des Télécommunications*, Tome 50, No. 7–8, 695–704, July–August 1995.
4. Morin, X., S. El Assad, and D. Barba, "Vector quantization of raw polarimetric SAR data by using their statistical properties," *Euro. Sym. on Satellite Remote Sensing III*, London, United Kingdom, September 1997.
5. Motet, J. C. and B. Marechal, "High resolution radar measurement of clutter," Colloque radar Paris, France, 534–539, May 1994.
6. Hamad, D. and S. El Assad, "Réseaux de neurones pour la visualisation plane de données multidimensionnelles," SFC'99, Nancy, France, September 1999.
7. El Assad, S., A. Saad, and D. Barba, "Segmentation markovienne vectorielle non supervisée d'images radar polarimétriques," *Traitement du Signal*, Vol. 14, No. 4, 405–421, 1997.
8. Read, C. J., D. V. Arnold, D. M. Chabries, and R. W. Christiansen, "A computation compression technique for SAR based on vector quantization," *IEEE 1988, National Radar Conference*, Vol. C, 91, April 1988.
9. Dutkiewicz, M. and I. Cumming, "Evaluation of the effects of

encoding on SAR data," *IEEE Photography Engineering and Remote Sensing*, Vol. 60, No. 7, 895–904, July 1994.

10. Chang, C. Y., R. Kwok, and J. C. Curlander, "Spatial compression of seasat SAR imagery," *IEEE Trans. on Geoscience and Remote Sensing*, Vol. 26, No. 5, September 1988.
11. Linde, Y. and R. M. Gray, "An algorithm for vector quantizer design," *IEEE Trans. on Communications*, 84–95, January 1980.
12. Kwok, R. and W. T. K. Johson, "Block adaptive quantization of Magellan SAR data," *IEEE Trans. on Geoscience and Remote Sensing*, Vol. 27, No. 4, July 1989.